

Cooperative dynamics in a class of coupled two-dimensional oscillators

J. A. Acebrón,* and W.-J. Rappel

Department of Physics, University of California, San Diego, La Jolla, California 92093

A. R. Bulsara

SPAWAR Systems Center Code D363, 49590 Lassing Road, RM A341 San Diego, California 92152-6147

(Received 19 April 2002; published 24 January 2003)

We study a system of globally coupled two-dimensional nonlinear oscillators [using the two-junction superconducting quantum interference device (SQUID) as a prototype for a single element] each of which can undergo a saddle-node bifurcation characterized by the disappearance of the stable minima in its potential energy function. This transition from fixed point solutions to spontaneous oscillations is controlled by external bias parameters, including the coupling coefficient. For the deterministic case, an extension of a center-manifold reduction, carried out earlier for the single oscillator, yields an oscillation frequency that depends on the coupling; the frequency decreases with coupling strength and/or the number of oscillators. In the presence of noise, a mean-field description leads to a nonlinear Fokker-Planck equation for the system which is investigated for experimentally realistic noise levels. Furthermore, we apply a weak external time-sinusoidal probe signal to each oscillator and use the resulting (classical) resonance to determine the underlying frequency of the noisy system. This leads to an explanation of earlier experimental results as well as the possibility of designing a more sensitive SQUID-based detection system.

DOI: 10.1103/PhysRevE.67.016210

PACS number(s): 05.45.-a, 05.40.Ca, 02.50.Ey, 02.30.Hq

I. INTRODUCTION

A large class of two-dimensional (2D) nonlinear systems, exemplified in this work by the two-junction or dc superconducting quantum interference device (SQUID), is known to display *spontaneous* (i.e., in the absence of external driving signals) oscillations when the dynamical system crosses a threshold through a bifurcation [1]. The oscillations are periodic but nonsinusoidal, approaching sinusoidal behavior as one goes farther past the bifurcation threshold. The oscillation frequency is a function of the “distance” past the onset of the bifurcation, and displays a characteristic scaling behavior with respect to the bias parameter that controls the bifurcation [1]. In specific dynamical systems, the spontaneous oscillation frequency may be computed, usually via a center-manifold reduction of the dynamics to a 1D normal form. Applying an external sinusoidal signal to the system in this state of spontaneous oscillation yields a very rich and complex dynamical behavior [2] including a lowering of the noise-floor (when fluctuations are present) as well as frequency-mixing behavior characterized by the generation of combination harmonics [3] whose spectral amplitudes depend on the background noise.

When tuned near the onset of bifurcations, dynamical systems can display an enhanced sensitivity to external perturbations with the response characterized by signal amplification [4], often with a concomitant lowering of an environmental noise floor (see, e.g., Refs. [2,5]), but also (depending on the parameters) potentially adverse effects, e.g., the amplification of environmental fluctuations with an

accompanying lowering of the response signal-to-noise ratio (SNR) [6]. Among the nonlinear systems that have been studied in recent years, the dc SQUID has recently received considerable attention, since it is a device that is severely constrained by noise-floor issues and one in which a detailed study of the (noise-mediated) cooperative behavior in various regimes of operation can yield clever techniques for confronting noise-related performance issues that constrain current devices.

The dc SQUID [7] consists of two Josephson junctions symmetrically inserted into a superconducting loop. It is the most sensitive magnetic field detector in existence and is widely used in a variety of fields including biomagnetics, geophysics, communications, and explosives detection. If no external signal is present, the system can be in either of two dynamical states depending on the biasing (usually achieved by a combination of externally applied magnetic flux and bias current to the SQUID loop): a static or superconducting state wherein the potential function has stable minima corresponding to a conservation of total loop current (the applied bias current is balanced by the sum of the Josephson currents in the junctions) and a spontaneously oscillating or “running” regime wherein the potential minima disappear. The oscillation (or running) frequency has been computed [8]; it shows the scaling behavior referred to above.

Past research has focused primarily on designing and developing sophisticated shielding and noise-cancellation techniques to render SQUIDs more noise tolerant and has, almost exclusively, dealt with single SQUIDs. Recently, a new strategy has emerged: instead of trying to minimize noise, this strategy searches for the area in parameter space where the SQUID is optimally sensitive. Specifically, the *stochastic resonance* (SR) effect [9] and its variations, have been studied theoretically [10,11] and experimentally [12], particularly

*Author to whom correspondence should be addressed. Email address: acebron@physics.ucsd.edu

near the onset of the saddle-node bifurcation from static to running dynamics. While the spectral response and the accompanying SNR at the frequency of a weak sinusoidal target signal have been observed in experiments [12] and simulations [10,11] to display a SR-like amplification, there are indications that this is not completely in line with the “classic” SR behavior. Specifically, we have observed a maximum in the SNR in the space of the *deterministic* control parameters (loop bias current and magnetic flux). The theory in this paper and in earlier work [13] provides an explanation for these experimental observations.

Often, a dramatic enhancement in the system response can be achieved by coupling elements in an array [14]. Motivated by this phenomenon, we study here the dynamical behavior in a globally coupled ensemble of dc SQUIDs with and without background noise (assumed to arise mainly from thermal fluctuations in the junctions). The SQUIDs and their bias conditions (including the coupling strengths) need not be identical in practice, although some restrictions may be imposed by our desire to obtain analytical results. We study our globally coupled system both analytically and numerically, finding that the system exhibits static and oscillatory regimes of operation, completely analogous to the single SQUID case [2,8]. Our analysis stems from the center-manifold reduction technique that was applied to the single SQUID problem, and recently described semianalytic techniques for solving the 2D Fokker-Planck equation (FPE) associated with the Langevin dynamics [15]. This previous work is conveniently generalized to treat the N -SQUID (N may be arbitrary) case with global coupling.

Particular attention is paid to the underlying (i.e., running) frequency of the system. For the deterministic case, we find an exact solution for the frequency of the running state. For the noisy case, however, a general technique to determine the frequency is not available. With small noise levels, a center-manifold reduction of the dynamics to a 1D normal form, as was performed in Ref. [8] is, in principle, possible (see also Ref. [16]). However, for experimentally realistic values of noise an alternative method needs to be applied. We have recently shown [13] that the introduction of a sinusoidal “probe” signal leads to a classical resonance phenomenon (also observed in Ref. [17] for a system undergoing a Hopf bifurcation) which can be exploited to determine the underlying frequency of the running state.

Our main results are the following.

(1) Increasing the number of SQUIDs renders the time-independent (superconducting) stationary state more stable, restricting the accessible values of the parameter where we can find an oscillatory solution.

(2) The frequency of the oscillatory solutions depends on the coupling, with large coupling and/or large N reducing the frequency and extending the parameter regime for the existence of stationary state; coupling can destroy the running solutions.

(3) A nonlinear FPE may be derived and solved in the stationary state for the averaged screening current, the relevant experimental observable. Notice that the Fokker-Planck equation obtained for a single element is always a linear partial differential equation (see, e.g., Ref. [18]). We stress

the fact that due to the nonlinear nature of our derived FPE classical results regarding linear FPEs including linear response theory [18,19] cannot be applied in general and alternative approaches are needed.

(4) Coupling a time-sinusoidal target or probe signal to each SQUID leads to a resonance in the averaged screening current when the signal frequency approaches the running frequency. This affords the possibility of using a single device or an array as a frequency-sensitive detector.

The paper is organized as follows: After a rapid overview of the dc SQUID dynamics in Sec. II, we obtain (Sec. III A) the stationary states and study the onset of the oscillatory regime in terms of the two natural laboratory control parameters, the magnetic flux Φ_{ex} , and the dc bias current J for arbitrary values of the coupling and number N of SQUIDs. In Sec. III B, we present an analytical calculation of the frequency of the running state and its scaling in terms of the distance from the bifurcation point. This is followed (Sec. IV) by an investigation into the effects of noise on the coupled system dynamics. Finally, we discuss the inclusion of a sinusoidal probe signal in Sec. V. Our results are summarized and discussed in Sec. VI.

II. BACKGROUND AND MODEL EQUATIONS

In its simplest form, a dc SQUID consists of two Josephson junctions inserted symmetrically (asymmetric configurations are also possible, in practice, but we do not treat this here) into a superconducting loop. The dynamics of this device are well known [7] and we offer only a rapid overview without derivation. In terms of the Schrödinger phase angles $\delta_{1,2}$ of the two (assumed identical) junctions we can write down the measurable screening current I in the loop,

$$\beta \frac{I}{I_0} = \delta_1 - \delta_2 - 2\pi \frac{\Phi_e}{\Phi_0} - 2\pi n, \quad (1)$$

where $\beta \equiv 2\pi L I_0 / \Phi_0$ is the nonlinearity parameter, I_0 is the junction critical current, L is the loop inductance, Φ_e is an external applied magnetic flux, and $\Phi_0 \equiv h/2e$ is the flux quantum. The quantum mechanical wave function along the superconducting loop must be single valued at any point in space. This can be accomplished if the magnetic flux is quantized which is ensured via the term containing the integer n . In the absence of noise and a target magnetic flux, we can use the resistively shunted junction model to write down equations for the currents in the two arms of the SQUID via a lumped circuit representation; when transformed via the Josephson relations $\delta_i = 2e V_i / \hbar$, linking the voltage and the quantum phase difference across the junction i , these equations take the form

$$\tau \delta_1 = \frac{I_b}{2} - I - I_0 \sin \delta_1, \quad \tau \delta_2 = \frac{I_b}{2} + I - I_0 \sin \delta_2, \quad (2)$$

where $\tau \equiv \hbar/2eR$, R being the normal state resistance of the junctions. The dc bias current I_b is applied symmetrically to

the loop. Rescaling the time by π/I_0 , one can write the above in the form $\dot{\delta}_i = -\partial U(\delta_1, \delta_2)/\partial \delta_i$ with the 2D potential function defined as

$$U(\delta_1, \delta_2) = -\cos \delta_1 - \cos \delta_2 - J(\delta_1 + \delta_2) + \frac{1}{2\beta}(\delta_1 - \delta_2 - 2\pi\Phi_{\text{ex}})^2, \quad (3)$$

where we have introduced the dimensionless bias current $J \equiv I_b/2I_0$ and normalized applied flux $\Phi_{\text{ex}} \equiv \Phi_e/\Phi_0$.

In the static regime, one may set the time derivatives in Eq. (2) equal to zero, in the absence of any external time-dependent signals; in practice, this could be done with time-dependent signals if the signal frequency as well as the bandwidth of any underlying noise are well contained within the device bandwidth τ^{-1} , ensuring that the device behaves like a static nonlinearity. The resultant steady-state phase equations are constrained by the continuity relation

$$\delta_2 - \delta_1 = 2\pi n - 2\pi \frac{\Phi_e + LI}{\Phi_0}. \quad (4)$$

Notice from Eqs. (2) and (1) that the screening current I is a periodic function in the applied magnetic flux Φ_{ex} , going through one complete cycle for every flux quantum Φ_0 applied. The inherent periodicity of the SQUID implies that it cannot distinguish between zero applied field and any other field that generates an integral number of flux quanta. Therefore, in the numerical simulations of our system of differential equations we have set $n=0$ for simplicity.

Adding and subtracting the steady-state phase equations, we are led immediately to the current conservation relations for the loop,

$$2J = \sin \delta_1 + \sin \delta_2, \quad 2I = I_0(\sin \delta_2 - \sin \delta_1). \quad (5)$$

Further, the I equation can be manipulated to yield a transcendental equation for the screening current,

$$\frac{I}{I_0} = -\sin\left(\pi\Phi_{\text{ex}} + \frac{\beta I}{2I_0}\right) \cos\left[\sin^{-1}\left(J + \frac{I}{I_0}\right) + \pi\Phi_{\text{ex}} + \frac{\beta I}{2I_0}\right]. \quad (6)$$

Equation (6) may be solved numerically for the screening current; the ensuing transfer characteristic (TC) is periodic in the applied flux Φ_{ex} with period 1, and possibly hysteretic, with the hysteresis loop width controlled by the bias current J . For $J=0$ one obtains hysteresis for any nonlinearity β ; for $0 < J \leq 1$, hysteresis occurs over some range of β , linked to a multistable potential function U . When the current conservation equations (5) are satisfied, the SQUID is in its superconducting state with the state point resting in a potential minimum, corresponding to a saturation state on the TC; in this configuration, the bias current is balanced by the Josephson supercurrents in the junctions.

A close examination of potential function (3) shows that the *externally adjustable* bias parameters Φ_{ex} and J control the symmetry and well depth, respectively. Adjusting these parameters leads to a transition from a regime characterized

by a multistable potential and the long-time static solutions discussed in the preceding paragraph, to one wherein pairs of minima and saddles have coalesced to yield a potential with points of inflection, followed by (upon further adjustment of the bias parameters) a potential with no minima. In this regime, the conservation relations are no longer obeyed unless one includes an ohmic correction term and the SQUID is said to be in the ‘‘running regime’’ (sometimes referred to as the ‘‘voltage regime’’), characterized by spontaneous oscillations in the observable (in this case, the screening current I). A ‘‘saddle-node’’ bifurcation has occurred with the critical point corresponding to a point of inflection in the potential. The spontaneous oscillations have zero frequency at the critical point; past this point, the frequency increases with a characteristic scaling behavior [1,8] with the distance from the bifurcation.

Following this preamble, we start with an extension of the model equations (2) to describe a system of globally linearly coupled dc SQUIDs, a network that can be experimentally realized in a variety of ways. One possible experimental scenario could be the following: a network of pickup coils is connected in parallel to sense and sum the fluxes of all the SQUIDs. Some of the resulting flux (depending on the coupling strength) is applied to each SQUID by feeding back the total output current through a feedback coil. Since every SQUID can interact magnetically with the next neighbor, leading to a local-type coupling, it is advisable to place each SQUID in a shielded environment. This form of coupling gives rise to a near-global coupling similar to the one we have proposed here, with each SQUID subject to a flux due to all the other SQUIDs in the same way. Global coupling is also most amenable (of all the possible coupling schemes) to theoretical treatment.

The theoretical variables of interest are the Schrödinger phase differences $\delta_j^{(k)}$ ($j=1,2$) across each Josephson junction of the k th SQUID ($k=1, \dots, N$),

$$\frac{\tau_k}{I_{0k}} \dot{\delta}_j^{(k)} = J_k + (-1)^j \frac{I_k}{I_{0k}} - \sin \delta_j^{(k)}, \quad j=1,2, \quad k=1, \dots, N, \quad (7)$$

where I_k represents the screening current, J_k the normalized (to I_{0k}) externally applied bias current, I_{0k} the critical current of the k th junctions, and $\tau_k = \hbar/(2eR_k)$ is a characteristic time constant (R_k being the normal state resistance of the junctions). The screening current I_k (the experimental observable of interest) at the k th SQUID is induced in the loop by an external magnetic flux Φ_e which is assumed identical for all SQUIDs. Each SQUID is inductively coupled to the loop currents of the remaining SQUIDs with equal mutual inductance coupling of strength M . The screening current can be written in the form

$$\beta_k \frac{I_k}{I_{0k}} = \delta_1^{(k)} - \delta_2^{(k)} - \frac{2\pi}{\Phi_0} \left(\Phi_e + M \sum_{m \neq k} I_m \right), \quad (8)$$

where $\beta_k \equiv 2\pi L_k I_{0k} / \Phi_0$ is the nonlinearity parameter of the k th SQUID, L_k being its loop inductance. Since the screening current I_m appearing on the right hand side of Eq. (8) is

itself a function of every other screening current, Eq. (8) represents an infinite nested series.

In general, this series cannot be summed in closed form; hence we expand in powers of M . To this end, let us rewrite Eq. (8) as $(A+B)I=\Delta$, where we define the following matrices:

$$A = \begin{bmatrix} \beta_1 & 0 & \cdots & 0 \\ 0 & \beta_2 & \cdots & 0 \\ \vdots & \ddots & \ddots & \vdots \\ 0 & \cdots & \cdots & \beta_N \end{bmatrix},$$

$$B = \frac{2\pi M}{\Phi_0} \begin{bmatrix} 0 & 1 & 1 & \cdots & 1 \\ 1 & 0 & 1 & \cdots & 1 \\ \vdots & & \ddots & \ddots & \vdots \\ 1 & 1 & 1 & \cdots & 0 \end{bmatrix}, \quad I = \begin{bmatrix} I_1/I_{01} \\ I_2/I_{02} \\ \vdots \\ I_N/I_{0N} \end{bmatrix},$$

$$\Delta = \begin{bmatrix} \delta_1^{(1)} - \delta_2^{(1)} - 2\pi\Phi_{ex} \\ \delta_1^{(2)} - \delta_2^{(2)} - 2\pi\Phi_{ex} \\ \vdots \\ \delta_1^{(N)} - \delta_2^{(N)} - 2\pi\Phi_{ex} \end{bmatrix}. \quad (9)$$

Then, we obtain by simple iteration,

$$I = A^{-1}\Delta \left[1 + \sum_{j=1}^{\infty} (-MBA^{-1})^j \right] = C\Delta, \quad (10)$$

where we have defined $C \equiv A^{-1}/(1 - MBA^{-1})$. For the special case of $N=2$, the sum in Eq. (10) can be performed analytically; the result is

$$I = \frac{1}{1 - \frac{4\pi^2 I_{01} I_{02}}{\Phi_0^2 \beta_1 \beta_2} M^2} \begin{bmatrix} \frac{I_{01}}{\beta_1} & -\frac{2\pi M}{\Phi_0} \frac{I_{01} I_{02}}{\beta_1 \beta_2} \\ -\frac{2\pi M}{\Phi_0} \frac{I_{01} I_{02}}{\beta_1 \beta_2} & \frac{I_{02}}{\beta_2} \end{bmatrix}. \quad (11)$$

Inserting Eq. (10) into Eq. (7), we arrive at our final set of equations for the dynamics of the k th SQUID,

$$\frac{\tau_k}{I_{0k}} \dot{\delta}_j^{(k)} = J_k + (-1)^j \sum_{i=1}^N C_{ki} (\delta_1^{(i)} - \delta_2^{(i)} - 2\pi\Phi_{ex}) - \sin \delta_j^{(k)},$$

$$j=1,2, \quad k=1, \dots, N. \quad (12)$$

III. GLOBALLY COUPLED SQUIDS WITHOUT NOISE

A. Onset of the running state

Before determining the onset of the running state for the coupled case, let us review the situation for a single SQUID. As mentioned earlier, a single dc SQUID exhibits two different states of operation: a superconducting state where the long-time phases are time independent, and a “running

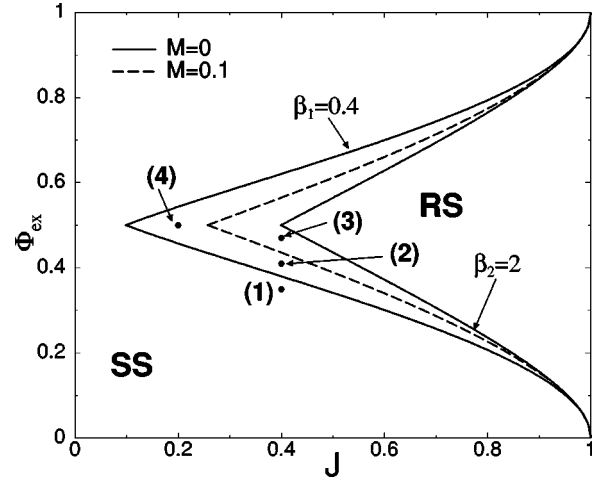


FIG. 1. Phase diagram in the parameter space (J, Φ_{ex}) of two different SQUIDS ($\beta_1=0.4, \beta_2=2$). SS denotes the stationary (i.e., superconducting) solution, while RS corresponds to the running state regime. The solid curves correspond to the uncoupled case ($M=0$), and the dashed curve to the coupled one ($M=0.1$). The screening current in the β_1 SQUID as a function of time is numerically calculated and displayed in Fig. 2 at the points marked by (1) $J=0.4, \Phi_{ex}=0.35$; (2) $J=0.4, \Phi_{ex}=0.41$; (3) $J=0.4, \Phi_{ex}=0.47$; and (4) $J=0.2, \Phi_{ex}=0.5$.

state” characterized by oscillatory phases. The boundary between these states is plotted for two different values of β in Fig. 1 (solid curves). The phase space in Fig. 1 is spanned by the two primary experimentally controllable parameters: the bias current J and the normalized external flux Φ_{ex} . Since our equations are invariant under $\Phi_{ex} \rightarrow 1 - \Phi_{ex}$ the phase diagram is symmetric around the $\Phi_{ex} = 1/2$ line. The region in phase space which exhibits the running state is labeled RS and the superconducting regime corresponds to SS. In the superconducting state, all solutions of Eq. (2) approach a fixed point, with the potential energy having stable minima corresponding to the current conservation $f = \sin \delta_1 + \sin \delta_2 - 2J$. In this state we can distinguish between two different cases: In the first one, the so-called hysteretic regime case, the system possesses four fixed points of which two are stable (nodes) and two are unstable (saddles). This case occurs for any value of the nonlinearity β when $J=0$, and occurs over some range of β when J is different from zero. In the second case, the system possesses only two fixed points, one stable and one unstable. The running state can be reached by increasing J and keeping Φ_{ex} constant. In both the hysteretic case and the nonhysteretic case the stable and unstable fixed points coalesce in a saddle-node bifurcation at $J=J_c$. Past J_c , a limit cycle is created in a global bifurcation, the attractor resulting from the chain of (merged) saddle-node-saddle connections [20].

The phase diagram (for a single SQUID, $M=0$) of Fig. 1 can obviously be obtained numerically; however, recent work [10] has shown that it can also be found analytically. Consider the function $f = \sin \delta_1 + \sin \delta_2 - 2J$. In the superconducting state a plot of f vs δ_1 will have two or four zeros (hysteretic or nonhysteretic regime, respectively). At the on-

set of the running state only one zero survives and f will have a maximum. Since δ_2 is given by the continuity equation $J - (\delta_2 - \delta_1 - 2\pi\Phi_{ex})/\beta - \sin \delta_1 = 0$ [obtained from the system (2) in the long-time limit], the onset of the running state can be found using the Lagrange multiplier technique: maximize f subject to the condition $J - (\delta_2 - \delta_1 - 2\pi\Phi_{ex})/\beta - \sin \delta_1 = 0$. The phase diagram so obtained [10] shows very good agreement with experimental results [12].

We can generalize this idea to the case of N SQUIDS. Without loss of generality we assume that $\beta_1 < \beta_2 < \dots < \beta_N$. We start with the uncoupled case, using earlier results [10] to obtain the critical point for each SQUID; specifically, we find the critical values of the bias current, J_{ck} , for fixed Φ_{ex} . For our particular choice of β_k we find that $J_{c1} < J_{c2} < \dots < J_{cN}$. As in the single SQUID case, we seek extrema of the function f , now defined for the first SQUID: $f_1 = \sin \delta_1^{(1)} + \sin \delta_2^{(1)} - 2J$, where we have assumed, for simplicity, identically biased SQUIDS, $J_k = J$ for all k . Rather than having a single constraint we now have $2N - 1$ constraints given by

$$L_i = J - \sin \delta_1^{(i)} + \sin \delta_1^{(i)} - 2J + \sum_{j=1}^N C_{ij}(\delta_1^{(j)} - \delta_2^{(j)} - 2\pi\Phi_{ex}),$$

$$i = 1, \dots, N, \quad (13)$$

$$K_i = -2J + \sin \delta_1^{(i)} + \sin \delta_2^{(i)}, \quad i = 2, \dots, N. \quad (14)$$

To find the extrema of f_1 , subject to the constraints L_i, K_i , we apply the Lagrange multiplier technique and construct the function

$$H(\delta_1^{(1)}, \delta_2^{(1)}; \dots; \delta_1^{(N)}, \delta_2^{(N)}) = f_1 + \sum_{i=1}^N \lambda_i L_i + \sum_{i=2}^N \lambda_{i+N-1} K_i. \quad (15)$$

The extrema of H , $\partial H / \partial \delta_{1,2}^{(i)} = 0$, $i = 1, \dots, N$, can be found by solving the following system of equations:

$$\frac{\partial H}{\partial \delta_1^{(1)}} = \cos \delta_1^{(1)} - \lambda_1(C_{11} + \cos \delta_1^{(1)}) - \sum_{i=2}^N C_{i1} \lambda_i = 0, \quad (16)$$

$$\frac{\partial H}{\partial \delta_1^{(2)}} = -\lambda_2(C_{22} + \cos \delta_1^{(2)}) - \sum_{i \neq 2} C_{i1} \lambda_i + \lambda_{N+1} \cos \delta_1^{(2)} = 0, \quad (17)$$

⋮

$$\frac{\partial H}{\partial \delta_1^{(N)}} = -\sum_{i=1}^{N-1} C_{iN} \lambda_i - \lambda_N(C_{22} + \cos \delta_1^{(N)}) + \lambda_{2N-1} \cos \delta_1^{(N)} = 0, \quad (18)$$

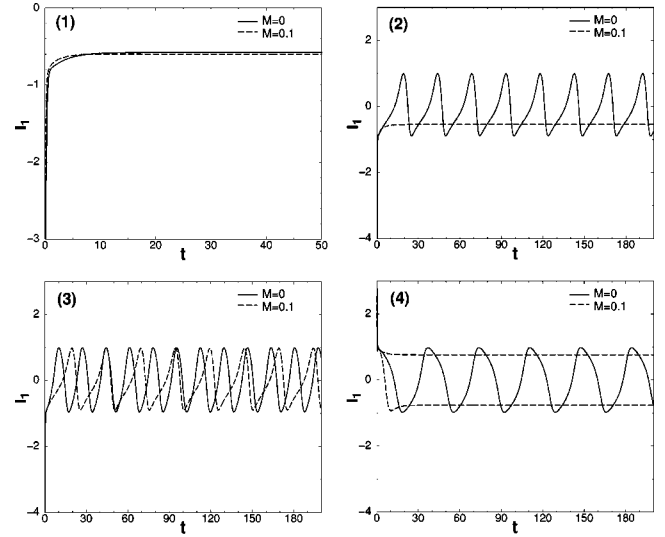


FIG. 2. Screening current of the β_1 SQUID, I_1 , as function of time for the coupled ($N=2$) and uncoupled case. Figures represent the points (1)–(4) on the phase diagram Fig. 1. In (4), for the coupled case, the evolution of two different initial conditions have been displayed, showing the existence of bistability (two solutions for $M=0.1$) of solutions. This corresponds to the hysteretic regime.

$$\frac{\partial H}{\partial \delta_2^{(1)}} = \cos \delta_2^{(1)} + \sum_{i=1}^N C_{i1} \lambda_i = 0, \quad (19)$$

$$\frac{\partial H}{\partial \delta_2^{(2)}} = \sum_{i=1}^N C_{i2} \lambda_i + \lambda_{N+1} \cos \delta_2^{(2)} = 0, \quad (20)$$

$$\vdots \quad (21)$$

$$\frac{\partial H}{\partial \delta_2^{(N)}} = \sum_{i=1}^N C_{iN} \lambda_i + \lambda_{2N-1} \cos \delta_2^{(N)} = 0. \quad (22)$$

λ_1 can be easily obtained, by summing Eqs. (16) and (20),

$$\lambda_1 = 1 + \frac{\cos \delta_2^{(1)}}{\cos \delta_1^{(1)}}, \quad (23)$$

while the other multipliers λ_i , $i = 2, \dots, 2N - 1$, are obtained by solving the corresponding linear system of equations. Once we eliminate the Lagrange multiplier λ_i , we obtain a single equation for $\delta_1^{(i)}$, $i = 1, \dots, N$. This set of equations, along with $L_i = 0$, $i = 1, \dots, N$, and $K_i = 0$, $i = 2, \dots, N$ allow us to find the maximum of f_1 , which will depend on Φ_{ex} . In addition, we require that such a maximum should coincide with $f_1 = 0$ at the onset of the running state. This results in a system of nonlinear equations that can be solved. By selecting the appropriate solution one obtains the critical value of the external flux Φ_{ex} (up to an integer constant).

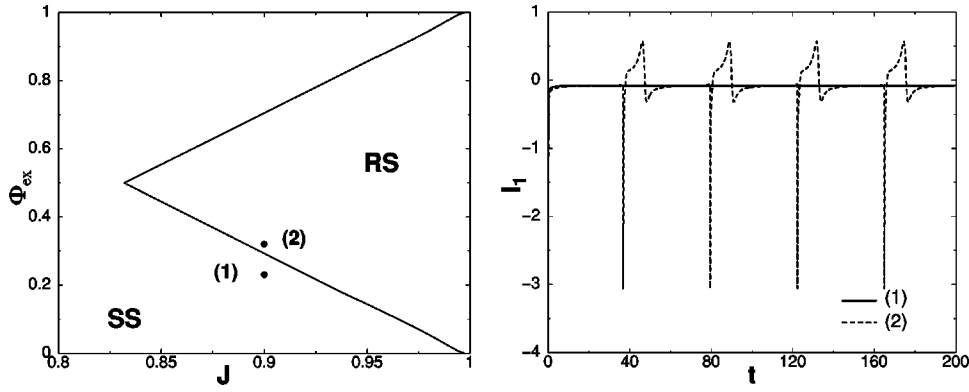


FIG. 3. Phase diagram in the parameter space (J, Φ_{ex}) of three different SQUIDS ($\beta_1=0.4, \beta_2=2, \beta_3=3$). The screening current of the β_1 SQUID, I_1 as a function of time is numerically calculated and displayed at the points marked by (1) $J=0.9, \Phi_{ex}=0.23$; and (2) $J=0.9, \Phi_{ex}=0.32$, for the coupled case ($M=0.1$).

In Fig. 1, we show the results of our calculation for $N=2$ as a dashed line. Since for this value of N we can sum Eq. (10) exactly, the boundary is exact. Figure 2 displays the time evolution of the screening current I_1 corresponding to the β_1 SQUID for the points marked (1) through (4) in Fig. 1. In Fig. 3 we show the phase diagram for three different coupled SQUIDS, and the screening current of the β_1 SQUID vs time is plotted. To obtain these results, we have summed Eq. (10) using ten terms. Our analytic results agree very well with numerical simulations, the relative error being less than 10^{-3} .

B. Frequency of the running state

Having found the locus of critical points for the onset of the running state we now proceed to find the frequency of the spontaneous oscillations. As in Sec. II A, we will make use of techniques applied to the single SQUID case [8]. For simplicity, we consider SQUIDS with identical critical current $I_{0k}=I_0$, normal resistance $R_k=R_0$, and identical bias ($J_k=J$). Rescaling time by τ/I_0 , Eqs. (7) and (10) yield

$$\dot{\delta}_j^{(k)} = J + \frac{(-1)^j}{\beta_k} \left[\delta_1^{(k)} - \delta_2^{(k)} - 2\pi\Phi_{ex} - \frac{2\pi}{\Phi_0} M \sum_{l \neq k} \frac{I_0}{\beta_l} (\delta_1^{(l)} - \delta_2^{(l)} - 2\pi\Phi_e) \right] - \sin \delta_j^{(k)} + O(M^2). \quad (24)$$

We start the analysis of the coupled case by considering the dynamics in the vicinity of the fixed-point solution when $J=J_{c1}$. It is convenient first to rewrite Eq. (24) in terms of the sum and difference variables $\Sigma^{(k)} = (\delta_1^{(k)} + \delta_2^{(k)})/2$, $\delta^{(k)} = (\delta_1^{(k)} - \delta_2^{(k)})/2$. Expanding Eq. (24) up to $O((J-J_{c1})^3)$ around the fixed-point solution $\Sigma_0^{(k)}, \delta_0^{(k)}$, and $J=J_{c1}$ yields

$$\dot{x}^{(k)} = - \left(\frac{2}{\beta_k} + A_k \right) x^{(k)} + B_k y^{(k)} + \frac{\varepsilon}{\beta_k} \sum_{j \neq k} \frac{1}{\beta_j} (2\delta_0^{(j)} - 2\pi\Phi_{ex}) + 2\varepsilon \sum_{j \neq k} x^{(j)} + C_k (x^{(k)})^2 + 2D_k x^{(k)} y^{(k)} + C_k (x^{(k)})^2,$$

$$\begin{aligned} \dot{y}^{(k)} &= (J - J_{c1}) - A_k y^{(k)} + B_k x^{(k)} + D_k (y^{(k)})^2 + 2C_k x^{(k)} y^{(k)} \\ &\quad + D_k (x^{(k)})^2, \\ J &= 0, \\ \dot{M} &= 0, \end{aligned} \quad (25)$$

where $x^{(k)} = \delta^{(k)} - \delta_0^{(k)}$, $y^{(k)} = \Sigma^{(k)} - \Sigma_0^{(k)}$, $A_k = \cos \Sigma_0^{(k)} \cos \delta_0^{(k)}$, $B_k = \sin \Sigma_0^{(k)} \sin \delta_0^{(k)}$, $C_k = (1/2) \cos \Sigma_0^{(k)} \sin \delta_0^{(k)}$, $D_k = (1/2) \sin \Sigma_0^{(k)} \cos \delta_0^{(k)}$, and we have introduced a rescaled coupling parameter $\varepsilon = 2\pi M / \Phi_0$.

To analyze the center manifold [20], the linear part must first be diagonalized. To this end, let us consider the following rotation:

$$\begin{bmatrix} v_1 \\ u_1 \\ \vdots \\ v_N \\ u_N \end{bmatrix} = S \begin{bmatrix} y_1 \\ x_1 \\ \vdots \\ y_N \\ x_N \end{bmatrix},$$

$$S = \begin{bmatrix} \cos \theta_1 & -\sin \theta_1 & 0 & 0 \cdots & 0 & 0 \\ \sin \theta_1 & \cos \theta_1 & 0 & 0 \cdots & 0 & 0 \\ \vdots & & \ddots & & \vdots & \\ 0 & 0 & 0 & 0 \cdots & \cos \theta_N & -\sin \theta_N \\ 0 & 0 & 0 & 0 \cdots & \sin \theta_N & \cos \theta_N \end{bmatrix}, \quad (26)$$

where $\tan 2\theta_k = -\beta_k \sin \Sigma_0^{(k)} \cos \delta_0^{(k)}$. The eigenvalues are given by

$$0, -\frac{2}{\beta_1} - 2A_1, -\frac{1}{\beta_k} - A_k \pm \frac{1}{\beta_k} \frac{1}{\cos 2\theta_k}, \quad k=2, \dots, N. \quad (27)$$

Using the transformation (26), Eq. (25) transforms into

$$\begin{aligned}
 \begin{bmatrix} \dot{v}_1 \\ \dot{u}_1 \\ \vdots \\ \dot{v}_N \\ \dot{u}_N \end{bmatrix} &= S \begin{bmatrix} J-J_{c1} \\ 0 \\ \vdots \\ J-J_{c1} \\ 0 \end{bmatrix} + S \begin{bmatrix} 0 \\ \frac{\varepsilon}{\beta_1} \sum_{j \neq 1} \frac{1}{\beta_j} (2\delta_0^{(j)} - 2\pi\Phi_{ex}) \\ \vdots \\ 0 \\ \frac{\varepsilon}{\beta_N} \sum_{j \neq N} \frac{1}{\beta_j} (2\delta_0^{(j)} - 2\pi\Phi_{ex}) \end{bmatrix} \quad (28) \\
 + \begin{bmatrix} 0 & 0 & 0 & 0 \cdots & 0 & 0 \\ 0 & -\frac{2}{\beta_1} - 2A_1 & 0 & 0 \cdots & 0 & 0 \\ \vdots & & \ddots & & \vdots & \\ 0 & 0 & 0 & 0 \cdots & \psi_{-N} & 0 \\ 0 & 0 & 0 & 0 \cdots & 0 & \psi_N \end{bmatrix} \begin{bmatrix} v_1 \\ u_1 \\ \vdots \\ v_N \\ u_N \end{bmatrix} + S \begin{bmatrix} D_1(y^{(1)})^2 + 2C_1x^{(1)}y^{(1)} + D_1(x^{(1)})^2 \\ 2\varepsilon \sum_{j \neq 1} x^{(j)} + C_1(x^{(1)})^2 + 2D_1x^{(1)}y^{(1)} + C_1(x^{(1)})^2 \\ \vdots \\ D_N(y^{(N)})^2 + 2C_Nx^{(N)}y^{(N)} + D_N(x^{(N)})^2 \\ 2\varepsilon \sum_{j \neq N} x^{(j)} + C_N(x^{(N)})^2 + 2D_Nx^{(N)}y^{(N)} + C_N(x^{(N)})^2 \end{bmatrix}, \quad (29)
 \end{aligned}$$

where $\psi_{\pm k} = -1/\beta_k - A_k \pm (1/\beta_k)(1/\cos 2\theta_k)$. It can be proven numerically that the eigenvalues are always negative or zero. Thus, from center-manifold theory, the stability of $(\Sigma^{(k)}, \delta^{(k)}) = (\Sigma_0^{(k)}, \delta_0^{(k)})$ near $J = J_{c1}$ can be determined by studying a one-parameter family of first-order ordinary differential equations on a center manifold, represented by the v_1 , and ε variables. To compute the center manifold and derive the vector field on the center manifold, we assume

$$\begin{aligned}
 u_i &= h_i(v_1, \varepsilon) = a_i^{(1)}v_1^2 + a_i^{(2)}\varepsilon v_1 + a_i^{(3)}\varepsilon^2 + \cdots, \\
 i &= 1, \dots, N, \quad (30)
 \end{aligned}$$

$$\begin{aligned}
 v_j &= h_{j+N}(v_1, \varepsilon) = b_j^{(1)}v_1^2 + b_j^{(2)}\varepsilon v_1 + b_j^{(3)}\varepsilon^2 + \cdots, \\
 j &= 2, \dots, N. \quad (31)
 \end{aligned}$$

The center manifold must satisfy [20]

$$f \frac{\partial h_i}{\partial v_1} - B_i h_i - g_i = 0, \quad i = 1, \dots, 2N-1, \quad (32)$$

where $f = D_1(y^{(1)})^2 + 2C_1x^{(1)}y^{(1)} + D_1(x^{(1)})^2$,

$$B = \begin{bmatrix} -\frac{2}{\beta_1} - 2A_1 \\ \psi_{-2} \\ \psi_2 \\ \vdots \\ \psi_{-N} \\ \psi_N \end{bmatrix},$$

$$g = \begin{bmatrix} 2\varepsilon \sum_{j \neq 1} x^{(j)} + C_1(x^{(1)})^2 + 2D_1x^{(1)}y^{(1)} + C_1(x^{(1)})^2 \\ \vdots \\ D_N(y^{(N)})^2 + 2C_Nx^{(N)}y^{(N)} + D_N(x^{(N)})^2 \\ 2\varepsilon \sum_{j \neq N} x^{(j)} + C_N(x^{(N)})^2 + 2D_Nx^{(N)}y^{(N)} + C_N(x^{(N)})^2 \end{bmatrix}. \quad (33)$$

From Eq. (32), equating terms of like powers to zero, the coefficients $a_i^{(l)}, b_j^{(l)}$ in expansion (31) can be obtained. Once such coefficients are found, the evolution of v_1 on the center manifold can be readily calculated as

$$\begin{aligned}
 \dot{v}_1 &= (J - J_{c1}) \cos \theta_1 - \left[\frac{\varepsilon}{\beta_1} \sum_{j=2}^N \frac{1}{\beta_j} (2\delta_0^{(j)} - 2\pi\Phi_{ex}) \right] \\
 &\times \sin \theta_1 + \alpha v_1^2 + 2\gamma \frac{\varepsilon^2}{\beta_1} v_1 + O((J - J_{c1})^3), \quad (34)
 \end{aligned}$$

where $\eta_j = (2/\psi_j) \cos \theta_j \sin \theta_1$, $\xi_j = [2/(\psi_{-j})] \sin \theta_j \sin \theta_1$, $\alpha = \cos \theta_1 (D_1 - C_1 \sin 2\theta_1) - \sin \theta_1 (C_1 - D_1 \sin 2\theta_1)$, and $\gamma = [\sum_{j=2}^N (1/\beta_j) (\xi_j \cos \theta_j \sin \theta_1 - \eta_j \sin \theta_j \sin \theta_1)]$. Integrating the last equation, we obtain the solution

$$v_1(t) = \sqrt{\frac{F}{\alpha} - \frac{\gamma^2 \varepsilon^4}{\alpha^2}} \tan(t \sqrt{F\alpha - \gamma^2 \varepsilon^4}) - \frac{\gamma \varepsilon^2}{\alpha}, \quad (35)$$

where $F = (J - J_{c1}) \cos \theta_1 - [(\varepsilon/\beta_1) \sum_{j=2}^N (1/\beta_j) (2\delta_0^{(j)} - 2\pi\Phi_{ex})] \sin \theta_1$. Thus, for the frequency of the running state we find

$$f = \sqrt{F\alpha - \gamma^2 \varepsilon^4} / 2\pi. \quad (36)$$

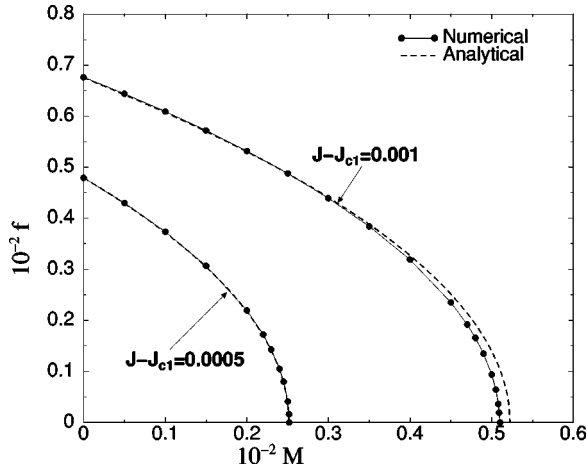


FIG. 4. Two SQUIDS: Comparison between the numerical simulations of the system of equations (7) and the analytical frequency for two different values of the bias current J : (1) $J = J_{c1} + 0.001$ and (2) $J = J_{c1} + 0.0005$, with $J_{c1} = 0.821152$. Parameters are $\beta_1 = 0.9$, $\beta_2 = 1$, and $\Phi_{ex} = 0.2$.

The most salient feature of this expression is that the frequency of the running state decreases when the coupling ε increases. In fact, there exists a critical value of the coupling [obtained by setting the right hand side of Eq. (36) equal to zero] above which the oscillation frequency is zero: too strong a coupling “kills” the running states. Thus, the coupling strength can be used to tune the system towards the bifurcation point, a feature we will use below when we discuss ways to improve SQUID sensitivity. Also, we have numerically verified that increasing the number N of SQUIDS results in a decrease in the frequency.

Figure 4 shows a comparison between the numerical simulations of the system of equations (7) and the frequency obtained by using the analytical expression (36) for the case of $N=2$. The agreement between the numerical results and the analytical results is excellent, particularly, as expected, for small values of $J - J_{c1}$. Figure 5 shows a similar comparison for the cases $N=3$ and $N=4$.

IV. GLOBALLY COUPLED SQUIDS WITH NOISE

In this section, we analyze the model equations (24) in presence of thermal noise. Specifically, we investigate the Langevin dynamics

$$\begin{aligned} \dot{\delta}_j^{(k)} = & J + \frac{(-1)^j}{\beta_k} \left[\delta_1^{(k)} - \delta_2^{(k)} - 2\pi\Phi_{ex} - \frac{2\pi}{\Phi_0} M \sum_{l \neq k} \frac{I_0}{\beta_l} (\delta_1^{(l)} \right. \\ & \left. - \delta_2^{(l)} - 2\pi\Phi_{ex}) \right] - \sin \delta_j^{(k)} + \xi_k^{(j)} + O(M^2), \end{aligned} \quad (37)$$

where $\xi_i^{(j)}$'s are Gaussian white noises, with $\langle \xi_i^{(j)}(t) \rangle = 0$, $\langle \xi_i^{(l)}(t) \xi_j^{(m)}(t') \rangle = 2D \delta_{ij} \delta_{lm} \delta(t - t')$.

Taking into account the mean-field-type coupling, the model (24) can be written in a more convenient form by defining the average screening current \bar{I} ,

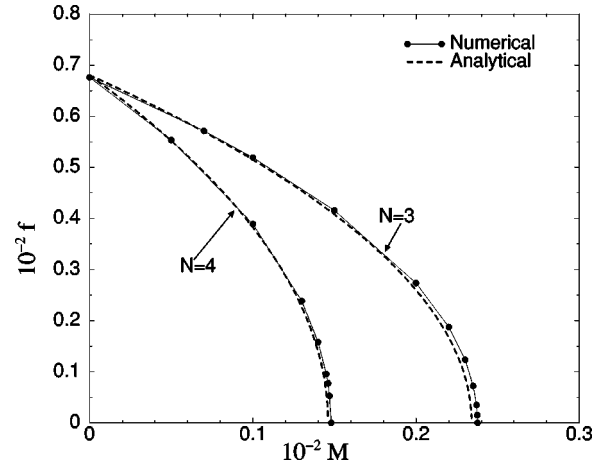


FIG. 5. Comparison between the numerical simulations of the system of equations (7), and the analytical frequency for $N=3$ and $N=4$ SQUIDS, kept fixed the bias current to $J = J_{c1} + 0.001$. Parameters are the same as in Fig. 4, and now $\beta_3 = 1.1$, and $\beta_4 = 1.3$.

$$\bar{I} = \frac{1}{N} \sum_{l=1}^N \frac{I_0}{\beta_l} \left(\delta_1^{(l)} - \delta_2^{(l)} - \frac{2\pi}{\Phi_0} \Phi_{ex} \right). \quad (38)$$

Then Eq. (37) reads

$$\begin{aligned} \dot{\delta}_j^{(k)} = & J + \frac{(-1)^j}{\beta_k} \left[\left(1 + \frac{2\pi}{\Phi_0 \beta_k} \frac{\bar{M} I_0}{N} \right) (\delta_1^{(k)} - \delta_2^{(k)} - 2\pi\Phi_{ex}) \right. \\ & \left. - \frac{2\pi}{\Phi_0} \bar{M} \bar{I} \right] - \sin \delta_j^{(k)} + \xi_k^{(j)} + O(M^2), \end{aligned} \quad (39)$$

where $\bar{M} \equiv MN$. We are interested in the analytical investigation of the Langevin dynamics above, for the case of very large N . A neat picture of such a case can be given by the limiting model obtained when $N \rightarrow \infty$ (thermodynamic limit). In this limit, it is well known [21,22] that models with mean-field coupling are described by an evolution equation for the one-particle probability density. This can be seen by noting that the hierarchy of equations for all the multiparticle probability densities can be closed by assuming molecular chaos. In such a way, the one-system probability density $\rho(\delta_1, \delta_2, t)$ is asymptotically in the limit, $N \rightarrow \infty$, the solution of the following *nonlinear* Fokker-Planck equation:

$$\frac{\partial \rho}{\partial t} = D \left[\frac{\partial^2 \rho}{\partial \delta_1^2} + \frac{\partial^2 \rho}{\partial \delta_2^2} \right] - \frac{\partial}{\partial \delta_1} (v_1 \rho) - \frac{\partial}{\partial \delta_2} (v_2 \rho). \quad (40)$$

The drift terms are given by

$$v_1(\delta_1, \delta_2, t) = J - \frac{1}{\beta} \eta(\delta_1, \delta_2) - \sin \delta_1, \quad (41)$$

$$v_2(\delta_1, \delta_2, t) = J + \frac{1}{\beta} \eta(\delta_1, \delta_2) - \sin \delta_2, \quad (42)$$

where $\eta = \delta_1 - \delta_2 - 2\pi\Phi_{ex} - (2\pi\bar{M}/\Phi_0)\bar{I}$.

The probability density is required to be 2π periodic as a function of δ_1 , and δ_2 , and normalized according to

$$\int_0^{2\pi} \int_0^{2\pi} \rho(\delta_1, \delta_2, t) d\delta_1 d\delta_2 = 1. \quad (43)$$

In order to satisfy the periodic boundary conditions, the coefficients appearing in the drift terms (41), (42) must be periodic, and the function $\eta(\delta_1, \delta_2)$ should be continued periodically as well. On the other hand, to satisfy the flux periodicity in the screening current, and reproduce the behavior found in Eq. (6) for a single element, the flux $2\pi\Phi_{ex}$

and coupling term $(2\pi\bar{M}/\Phi_0)\bar{I}$ should also be periodic. Then, the expression for η is

$$\begin{aligned} \eta &= \delta_1 - \delta_2 - 2\pi\Phi_{ex} - (2\pi\bar{M}/\Phi_0)\bar{I} \\ &= i \sum_{l=1}^{\infty} \frac{(-1)^l}{l} [e^{i l [\delta_1 - \delta_2 - 2\pi\Phi_{ex} - (2\pi\bar{M}/\Phi_0)\bar{I}]} \\ &\quad - e^{-i l [\delta_1 - \delta_2 - 2\pi\Phi_{ex} - (2\pi\bar{M}/\Phi_0)\bar{I}]}]. \end{aligned} \quad (44)$$

The average screening current is now given by

$$\bar{I}(t) = I_0 \int d\beta f(\beta) \int dJ g(J) \int d\Phi_{ex} h(\Phi_{ex}) \int_0^{2\pi} \int_0^{2\pi} d\delta_1 d\delta_2 \frac{1}{\beta} \eta'(\delta_1, \delta_2) \rho(\delta_1, \delta_2, t), \quad (45)$$

where $\eta'(\delta_1, \delta_2)$ is the periodic continuation of $\delta_1 - \delta_2 - 2\pi\Phi_{ex}$. For completeness, we have allowed for the possibility that the parameter values β , J , and Φ_{ex} may be drawn from distributions $f(\beta)$, $g(J)$, and $h(\Phi_{ex})$, respectively. However, for simplicity, we will restrict ourselves to identical SQUIDs in the remainder of the paper. As in other systems of coupled stochastic equations [23], the FPE derived here is nonlinear which can be easily seen by inserting Eq. (45) into Eq. (40). Thus, in contrast to the single SQUID case [15], where the FPE is linear, we can expect more complicated dynamical behavior.

For the special case $J=0$, it is possible to find an analytical solution for long time, assuming that a steady-state regime is reached. The stationary solution is given, in this case, by

$$\rho_0(\delta_1, \delta_2; \beta, \Phi_{ex}) = \alpha e^{-(1/2\beta D)\eta^2} e^{(1/D)\cos\delta_1} e^{(1/D)\cos\delta_2}, \quad (46)$$

where

$$\alpha = \left[\int_0^{2\pi} \int_0^{2\pi} d\delta_1 d\delta_2 e^{-(1/2\beta D)\eta^2} e^{(1/D)\cos\delta_1} e^{(1/D)\cos\delta_2} \right]^{-1}, \quad (47)$$

and

$$\begin{aligned} \bar{I} &= I_0 \int_0^{2\pi} \int_0^{2\pi} d\delta_1 d\delta_2 \frac{1}{\beta} (\delta_1 - \delta_2 - 2\pi n \\ &\quad - 2\pi\Phi_{ex}) \rho_0(\delta_1, \delta_2; \beta, \Phi_{ex}), \end{aligned} \quad (48)$$

where it should be noted that the average screening current \bar{I} in Eq. (46) is determined self-consistently via Eq. (48).

In order to study the solution of the FPE in more cases of interest, we have to invoke numerical simulations. To solve the nonlinear FPE, we utilize our recently developed numerical method, which consists of a generalization of the spectral

method (see, e.g., Ref. [18]) for a single SQUID already derived in Ref. [15]. The idea is to expand ρ in Fourier series,

$$\rho(\delta_1, \delta_2, t) = \sum_{n=-\infty}^{\infty} \sum_{m=-\infty}^{\infty} r_n^m(t) e^{i n \delta_1} e^{i m \delta_2}, \quad (49)$$

exploiting the 2π periodicity in δ_1 and δ_2 . The coefficients r_n^m in Eq. (49) are complex valued, while ρ is real valued. Thus, $r_n^m = (r_{-n}^{-m})^*$, where $*$ denotes the complex conjugate. From the normalization condition (43), it follows $r_0^0 = 1/(2\pi)^2$. Introducing Eq. (49) into the FPE, we obtain the following hierarchy of ordinary differential equations for the coefficients r_n^m :

$$\begin{aligned} \dot{r}_n^m &= -D(n^2 + m^2)r_n^m - iJ(n+m)r_n^m + \frac{n}{2}(r_{n-1}^m - r_{n+1}^m) \\ &\quad + \frac{m}{2}(r_n^{m-1} - r_n^{m+1}) \\ &\quad + \frac{n-m}{\beta} \sum_l \frac{(-1)^{l+1}}{l} \{ \cos[2\pi l(\Phi_{ex} + \bar{M}\bar{I})](r_{n-l}^{m+l} \\ &\quad - r_{n+l}^{m-l}) - i \sin[2\pi l(\Phi_{ex} + \bar{M}\bar{I})](r_{n-l}^{m+l} + r_{n+l}^{m-l}) \}, \\ n &= -\infty, \dots, \infty, \quad m = -\infty, \dots, \infty, \quad l = 1, \dots, \infty, \end{aligned} \quad (50)$$

where the average screening current \bar{I} is given by

$$\bar{I}(t) = \frac{I_0}{\beta} \left[8\pi^2 \sum_{l=1}^{\infty} \frac{(-1)^l}{l} \text{Im}(r_l^{-l} e^{i 2\pi l \Phi_{ex}}) \right]. \quad (51)$$

The numerical method consists of truncating the infinite hierarchy of first-order, coupled nonlinear differential equations, for a reasonable number of coefficients $n = -N, \dots, N$, and $m = -M, \dots, M$, setting $r_{N+1}^{M+1} = r_{-N-1}^{-M-1} = 0$. For the truncation of the system of infinitely many non-

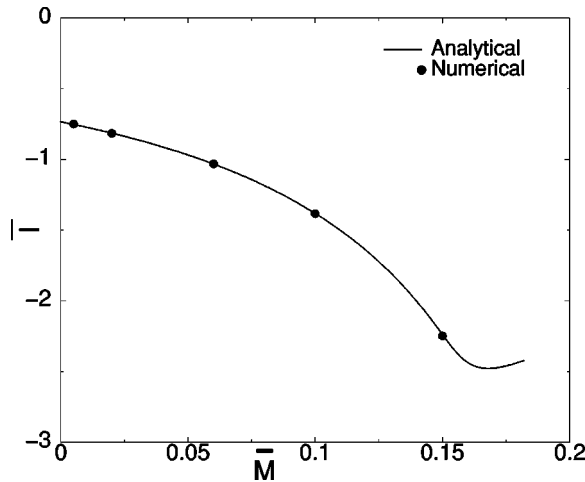


FIG. 6. Comparison between the average screening current \bar{I} obtained by solving numerically the nonlinear Fokker-Planck equation (spectral method), and the analytical solution for different values of the coupling strength \bar{M} . SQUIDs are identical, and parameters are $J=0$, $\beta=1$, $\Phi_{ex}=0.4$, and $D=0.1$.

linear ordinary differential equations some experimentation has been made, according to the following strategy: a number N , $2N$, $4N$ of coefficients has been used, and the choice of N (similarly with M) was made when the absolute error in ρ dropped below a given tolerance, typically 10^{-12} . The systems of ordinary differential equations have been solved by a variable step Runge-Kutta-Fehlberg scheme.

We have compared the numerical solution obtained via the nonlinear Fokker-Planck approach for a one-SQUID probability density, to the solution of the Langevin equations for a large number of SQUIDs ($N=500$). The solution of the FPE, corresponding to the limiting model (corresponding to $N \rightarrow \infty$) provides (not shown) excellent agreement with the N -finite case. This shows that $N=500$ is already close to infinity for a practical purpose. Finally, Fig. 6 shows a comparison between the analytical and numerical solutions of the FPE for the case $J=0$ for different values of the coupling parameter \bar{M} . The perfect agreement between the analytical and numerical results validates our numerical scheme.

V. INCLUSION OF AN EXTERNAL PROBE SIGNAL

A. Numerical results

For the deterministic case we have already found that the coupling strength changes the frequency of the running state. To investigate the effect of the coupling strength in the noisy case we need to determine the underlying frequency of the system. One way of determining this frequency is to compute \bar{I} from the Langevin equations and evaluate its time dependence. Unfortunately, this is computationally very costly. On the other hand, our extensive numerical investigations have shown that \bar{I} calculated from the FPE, which offers a computationally superior way to characterize the system, does not display a time-dependent behavior [24]. Of course, this finding does not rule out the existence of a stable

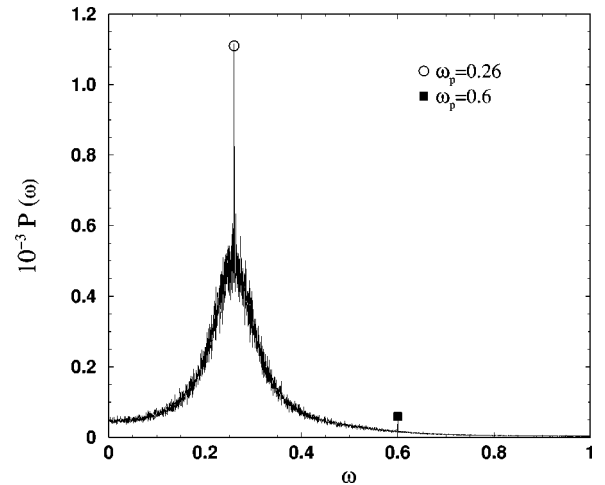


FIG. 7. Power spectra of the screening current for a flux-injected probe signal with $\omega_p=0.26$ and $\omega_p=0.6$. The peaks at the probe frequency are denoted by a solid square and open circle, respectively. Parameter values are $D=0.05$, $\beta=1$, $J=0.4$, $\Phi_e/\Phi_0=0.45$, $q=0.0025$, and $M=0.02$.

time-dependent solution, but does require an alternative way to find the frequency. Fortunately, as we will see below, including an external time-sinusoidal probe signal leads to a classical resonance (also observed in Ref. [17] for a system undergoing a Hopf bifurcation) which can be used to determine the underlying frequency.

We will consider an external flux that has a time-sinusoidal component (referred to in the figures, as the flux-injected probe signal): $\Phi_e = \Phi_e^{(0)} + q \sin(\omega_p t)$ and assume, for simplicity, that all the junctions have identical critical currents I_0 . As an aside, we mention here that we have obtained similar qualitative results when keeping the external flux constant and adding a sinusoidal component to the bias current (see the Appendix). To illustrate the effect of the probe signal, we first performed Langevin simulations for $N=2$ and calculated the average screening current \bar{I} . In Fig. 7 we have plotted the power spectrum of this quantity, for two different probe signals; one with a frequency ω_p that differs significantly from and one that is very close to the underlying frequency. The power spectrum was obtained by averaging 100 time series of 2^{23} time steps each. The figure illustrates clearly that for a probe signal frequency that matches the broad peak (corresponding to the, in-general, nonsinusoidal running oscillations) in the power spectrum of the unprobed system, the signal is amplified dramatically (open circle). Thus, adding a probe signal gives us a tool to investigate the dynamics of the noisy system.

To explore parameter space systematically let us now turn to the FPE. In Fig. 8, we have plotted an example of the result of a simulation of the FPE. It shows that \bar{I} becomes nearly purely sinusoidal when we include a sinusoidal probe signal after a transient. It also shows that the amplitude of the oscillations in \bar{I} , $A_{\bar{I}}$, is a function of ω_p . This is also illustrated in Fig. 9 where we show $A_{\bar{I}}^2/2$ (see below), for two

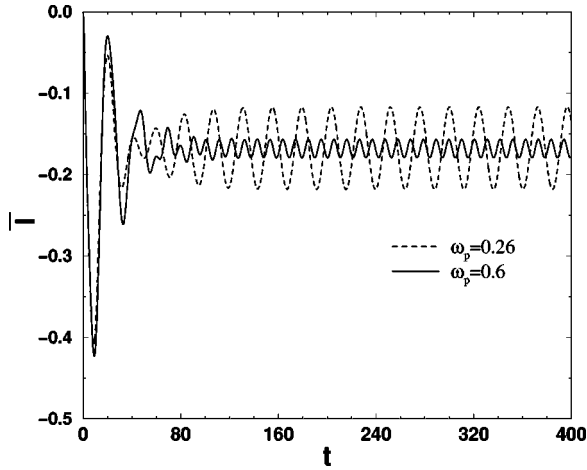


FIG. 8. Time evolution of the average screening current \bar{I} for two different values of the frequency of the flux-injected probe signal: $\omega_p=0.26$, $\omega_p=0.6$. Parameters are $D=0.05$, $\beta=1$, $J=0.4$, $\Phi_e^{(0)}=0.45$, and $q=0.01$.

different values of \bar{M} , as a function of ω_p . The appearance of a well defined peak in Fig. 9 demonstrates the classical resonance effect.

Of course, the FPE is strictly valid only for $N \rightarrow \infty$, however, we have seen that the Fokker-Planck approach already yields quantitatively correct answers for relatively small values of N . Furthermore, the qualitative behavior for $N=2$ and $N \rightarrow \infty$ is mostly the same. In particular, both limits display the characteristic resonance of Fig. 7. As a test of our simulations, we can compare the results obtained with the FPE to results obtained with the Langevin equations for large N . To

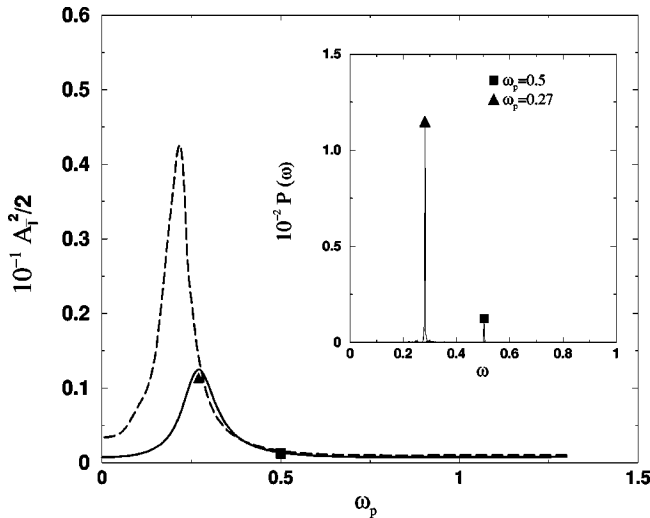


FIG. 9. $A_T^2/2$, obtained by solving the FPE, as a function of the flux-injected probe frequency for two different values of the coupling strength: $\bar{M}=0.01$ (solid line) and $\bar{M}=0.05$ (dashed line). The SQUIDs are identical, with $q=0.01$ and remaining parameters as in Fig. 8. The inset shows the power spectra obtained via direct Langevin simulations for $N=500$ for $\omega_p=0.5$ (square), and $\omega_p=0.27$ (triangle). The peaks of these power spectra are also plotted in the main figure.

this end, we calculated the power spectrum of \bar{I} as described above for $N=500$. The comparison is made easier by the fact that the output signal is essentially sinusoidal which allows us to relate $A_T^2/2$ to the peak in the power spectrum. This power spectrum, for two different values of ω_p , is shown in Fig. 9 as an inset. The peaks of these power spectrum are plotted as symbols in Fig. 9 and demonstrate that the FPE accurately describes the dynamics, at least for $N \geq 500$.

B. Towards a theory

Analytical progress can be made if we consider a small amplitude signal, $q = \varepsilon Q$, where $\varepsilon \ll 1$. Thus, Eq. (40) contains terms with two different time scales and can be analyzed via the method of multiple scales. It is then to be expected that an appropriate asymptotic method will be able to capture the long-time behavior of ρ . This may be achieved by introducing fast and slow time scales as follows:

$$\tau = \frac{t}{\varepsilon}, \quad t = t. \quad (52)$$

We look for a distribution function which is a 2π periodic function of δ_1 and δ_2 according to the ansatz,

$$\rho(\delta_1, \delta_2, t; \varepsilon) = \sum_{n=0}^2 \rho^{(n)}(\delta_1, \delta_2, t, \tau) \varepsilon^n + O(\varepsilon^3). \quad (53)$$

The expansion of the periodic function $h(\delta_1, \delta_2, \varepsilon) = (1/\beta) \times [\delta_1 - \delta_2 - 2\pi n - 2\pi(\Phi_e/\Phi_0)]$ in Eq. (42), where n is an integer that ensures the 2π periodicity of the solution, in powers of ε is given by

$$h = h(\delta_1, \delta_2, 0) + \varepsilon \left. \frac{dh}{d\varepsilon} \right|_{\varepsilon=0} + O(\varepsilon^2). \quad (54)$$

Taking into account that $\Phi_e = \Phi_e^{(0)} + \varepsilon Q \sin(\omega_p t)$, we find that

$$\left. \frac{dh}{d\varepsilon} \right|_{\varepsilon=0} = Q \sin(\omega_p t) \frac{d\nu}{d\Phi_e^{(0)}}, \quad (55)$$

where

$$\nu = \frac{1}{\beta} \left(\delta_1 - \delta_2 - 2\pi n - 2\pi \frac{\Phi_e^{(0)}}{\Phi_0} \right). \quad (56)$$

Inserting Eqs. (53), (54), and (55) into Eq. (40), we obtain the following hierarchy of equations for $\rho^{(j)}$:

$$\frac{\partial \rho^{(0)}}{\partial \tau} = 0, \quad (57)$$

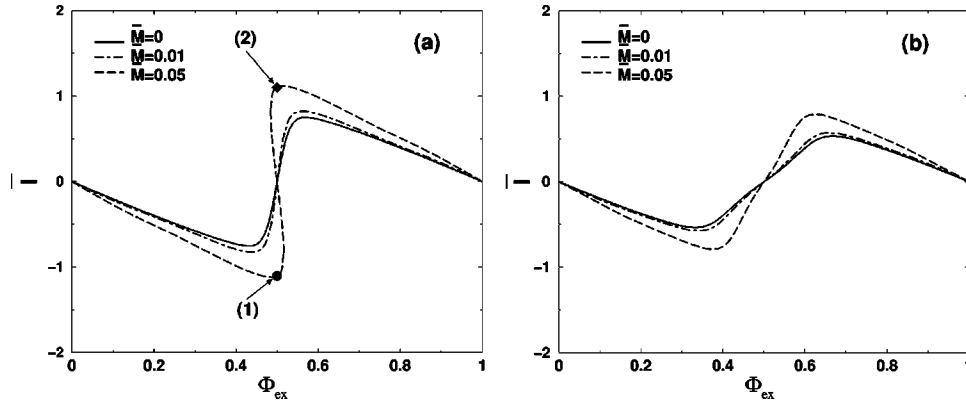


FIG. 10. Transfer characteristics for different coupling strength values, and for two different values of the bias current J [$J=0.1$ in (a), and $J=0.35$ in (b)]. In (a), the points marked by (1),(2) correspond to the solution obtained by numerical simulation of the FPE. Other parameters are $D=0.1$, and $\beta=1$.

$$\begin{aligned} \frac{\partial \rho^{(1)}}{\partial \tau} = & D \left[\frac{\partial^2 \rho^{(0)}}{\partial \delta_1^2} + \frac{\partial^2 \rho^{(0)}}{\partial \delta_2^2} \right] \\ & - \frac{\partial}{\partial \delta_1} \left[\left(J - \nu - \sin \delta_1 + \frac{2\pi \bar{M}}{\beta \Phi_0} \bar{I}^{(0)} \right) \rho^{(0)} \right] \\ & - \frac{\partial}{\partial \delta_2} \left[\left(J + \nu - \sin \delta_2 - \frac{2\pi \bar{M}}{\beta \Phi_0} \bar{I}^{(0)} \right) \rho^{(0)} \right] \\ & - \frac{\partial \rho^{(0)}}{\partial t}, \end{aligned} \quad (58)$$

$$\begin{aligned} \frac{\partial \rho^{(2)}}{\partial \tau} = & D \left[\frac{\partial^2 \rho^{(1)}}{\partial \delta_1^2} + \frac{\partial^2 \rho^{(1)}}{\partial \delta_2^2} \right] - \frac{\partial}{\partial \delta_1} \left[(J - \nu - \sin \delta_1) \rho^{(1)} \right. \\ & \left. + \frac{2\pi \bar{M}}{\beta \Phi_0} (\bar{I}^{(0)} \rho^{(1)} + \bar{I}^{(1)} \rho^{(0)}) \right] \\ & - \frac{\partial}{\partial \delta_2} \left[(J + \nu - \sin \delta_2) \rho^{(1)} - \frac{2\pi \bar{M}}{\beta \Phi_0} (\bar{I}^{(0)} \rho^{(1)} \right. \\ & \left. + \bar{I}^{(1)} \rho^{(0)}) \right] - \frac{\partial \rho^{(1)}}{\partial t} + Q \sin(\omega_p t) \\ & \times \left\{ \frac{\partial}{\partial \delta_1} \left[\frac{d\nu}{d\Phi_e^{(0)}} \rho^{(0)} \right] - \frac{\partial}{\partial \delta_2} \left[\frac{d\nu}{d\Phi_e^{(0)}} \rho^{(0)} \right] \right\}, \end{aligned} \quad (59)$$

where

$$\bar{I}^{(0)} = \int_0^{2\pi} \int_0^{2\pi} d\delta_1 d\delta_2 \nu \rho^{(0)}, \quad (60)$$

$$\bar{I}^{(1)} = \int_0^{2\pi} \int_0^{2\pi} d\delta_1 d\delta_2 \left(\nu \rho^{(1)} + Q \sin(\omega_p t) \frac{d\nu}{d\Phi_e^{(0)}} \rho^{(0)} \right). \quad (61)$$

The normalization conditions

$$\int_0^{2\pi} \int_0^{2\pi} \rho^{(n)}(\delta_1, \delta_2, t) d\delta_1 d\delta_2 = \delta_{0n} \quad (62)$$

follow from Eq. (43).

Equation (57) implies that $\rho^{(0)}$ is independent of τ . Then the terms in the right side of Eq. (58) which do not have τ -dependent coefficients give rise to secular terms (unbounded on the τ time scale). The condition that no secular terms should appear is

$$\begin{aligned} D \left[\frac{\partial^2 \rho^{(0)}}{\partial \delta_1^2} + \frac{\partial^2 \rho^{(0)}}{\partial \delta_2^2} \right] - \frac{\partial}{\partial \delta_1} \left[\left(J - \nu - \sin \delta_1 + \frac{2\pi \bar{M}}{\beta \Phi_0} \bar{I}^{(0)} \right) \rho^{(0)} \right] \\ - \frac{\partial}{\partial \delta_2} \left[\left(J + \nu - \sin \delta_2 - \frac{2\pi \bar{M}}{\beta \Phi_0} \bar{I}^{(0)} \right) \rho^{(0)} \right] - \frac{\partial \rho^{(0)}}{\partial t} = 0. \end{aligned} \quad (63)$$

This equation should be solved for $\rho^{(0)}$ together with Eq. (60), the normalization condition, and initial condition data. Note that this problem is equivalent to solving the FPE (40) without the probe signal. As mentioned above numerical experiments show that the solution of this FPE evolves towards a stationary state at long times. Such a stationary solution can be found by imposing $\dot{\rho}^m = 0$ in Eq. (50), and solving numerically the corresponding nonlinear system of equations. As in the single SQUID case [15], it is worthwhile to study the input-output transfer characteristic (TC), which is a convenient descriptor of the system response in terms of experimentally measurable quantities. The TC is a plot of the average screening current \bar{I} vs the external flux Φ_{ex} . In Fig. 10 we show the effect of the coupling strength on the TCs for two different values of the bias current. The TC is a periodic function in Φ_{ex} [see Eq. (50)], so only one complete cycle is shown for each J . Notice that in Fig. 10(a), a hysteretic behavior can be observed for large values of the coupling, and

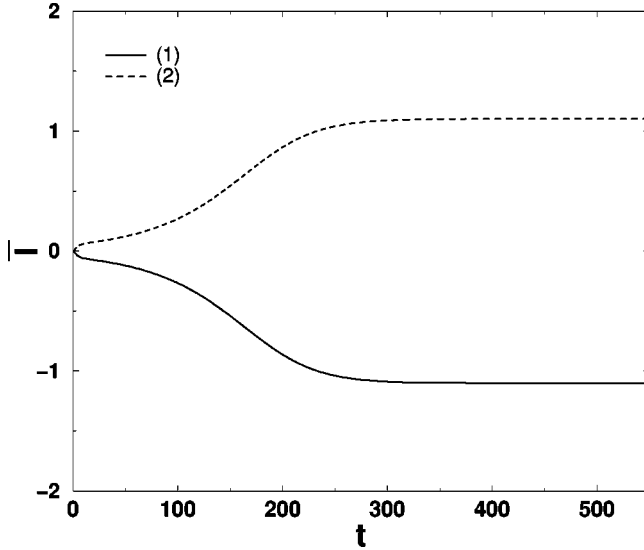


FIG. 11. Time evolution of the average screening current \bar{I} for two different initial conditions. Parameters are $D=0.1$, $J=0.1$, $\beta=1$, $\Phi_{ex}=0.5$, and $\bar{M}=0.05$ corresponding to the hysteresis regime in Fig. 10(a).

some range of J . The hysteresis is characterized by a negative slope of the transfer characteristic at $\Phi_{ex}=0.5$, showing three possible solutions. Only two of them, however, are stable, corresponding to the upper and lower branch. By increasing Φ_{ex} we can reach the upper branch for values of Φ_{ex} higher than 0.5, while the contrary takes place when we decrease Φ_{ex} . The branch connecting the upper and lower branch in Fig. 10(a) cannot be observed in the numerical simulations (see Fig. 11), and is therefore most likely unstable. This behavior can also be found in the noiseless single SQUID case [10]. Note that the effects of the probe signal are absent from the zero-order expression for the distribution function, $\rho^{(0)}$; they do appear when calculating the first correction, $\rho^{(1)}$.

To calculate first-order corrections, we again impose the condition that no secular terms appear and that the right-hand side of Eq. (59) vanishes. The resulting equation is

$$\begin{aligned}
 D \left[\frac{\partial^2 \rho^{(1)}}{\partial \delta_1^2} + \frac{\partial^2 \rho^{(1)}}{\partial \delta_2^2} \right] - \frac{\partial}{\partial \delta_1} \left[(J - \nu - \sin \delta_1) \rho^{(1)} \right. \\
 \left. + \frac{2\pi \bar{M}}{\beta \Phi_0} (\bar{I}^{(0)} \rho^{(1)} + \bar{I}^{(1)} \rho^{(0)}) \right] - \frac{\partial}{\partial \delta_2} \left[(J + \nu \right. \\
 \left. - \sin \delta_2) \rho^{(1)} - \frac{2\pi \bar{M}}{\beta \Phi_0} (\bar{I}^{(0)} \rho^{(1)} + \bar{I}^{(1)} \rho^{(0)}) \right] - \frac{\partial \rho^{(1)}}{\partial t} \\
 \left. + Q \sin(\omega_p t) \left\{ \frac{\partial}{\partial \delta_1} \left[\frac{d\nu}{d\Phi_e^{(0)}} \rho^{(0)} \right] - \frac{\partial}{\partial \delta_2} \left[\frac{d\nu}{d\Phi_e^{(0)}} \rho^{(0)} \right] \right\} \right] \\
 = 0. \tag{64}
 \end{aligned}$$

The analysis of the equation above can be readily accomplished in Fourier space. Fourier transforming Eq. (64), we obtain

$$\begin{aligned}
 i\omega \hat{\rho}^{(1)} = D \left[\frac{\partial^2 \hat{\rho}^{(1)}}{\partial \delta_1^2} + \frac{\partial^2 \hat{\rho}^{(1)}}{\partial \delta_2^2} \right] - \frac{\partial}{\partial \delta_1} \left[(J - \nu - \sin \delta_1) \hat{\rho}^{(1)} \right. \\
 \left. + \frac{2\pi \bar{M}}{\beta \Phi_0} (\hat{I}^{(0)*} \hat{\rho}^{(1)} + \hat{I}^{(1)*} \hat{\rho}^{(0)}) \right] - \frac{\partial}{\partial \delta_2} \left[(J + \nu \right. \\
 \left. - \sin \delta_2) \hat{\rho}^{(1)} - \frac{2\pi \bar{M}}{\beta \Phi_0} (\hat{I}^{(0)*} \hat{\rho}^{(1)} + \hat{I}^{(1)*} \hat{\rho}^{(0)}) \right] \\
 \left. + i \frac{Q}{2} \left\{ \frac{\partial}{\partial \delta_1} \left[\frac{d\nu}{d\Phi_e^{(0)}} [\hat{\rho}^{(0)}(\omega + \omega_p) - \hat{\rho}^{(0)}(\omega - \omega_p)] \right] \right. \right. \\
 \left. \left. - \frac{\partial}{\partial \delta_2} \left[\frac{d\nu}{d\Phi_e^{(0)}} [\hat{\rho}^{(0)}(\omega + \omega_p) - \hat{\rho}^{(0)}(\omega - \omega_p)] \right] \right\}, \tag{65}
 \end{aligned}$$

where

$$\hat{\rho}^{(j)}(\delta_1, \delta_2, \omega) = \int_{-\infty}^{\infty} dt e^{-i\omega t} \rho^{(j)}(\delta_1, \delta_2, t), \quad j=0,1, \tag{66}$$

$$\hat{I}^{(0)} = \int_0^{2\pi} \int_0^{2\pi} d\delta_1 d\delta_2 \nu \hat{\rho}^{(0)}, \tag{67}$$

$$\begin{aligned}
 \hat{I}^{(1)} = \int_0^{2\pi} \int_0^{2\pi} d\delta_1 d\delta_2 \left[\nu \hat{\rho}^{(1)} + i \frac{Q}{2} \frac{d\nu}{d\Phi_e^{(0)}} [\hat{\rho}^{(0)}(\omega + \omega_p) \right. \\
 \left. - \hat{\rho}^{(0)}(\omega - \omega_p)] \right], \tag{68}
 \end{aligned}$$

and * denotes convolution. Equation (65) should be solved for $\hat{\rho}^{(1)}$ together with $\int_0^{2\pi} \int_0^{2\pi} d\delta_1 d\delta_2 \hat{\rho}^{(1)} = 0$. Assuming that $\rho^{(0)}$ evolves to a stationary solution for long time [i.e., $\hat{\rho}^{(0)} = \delta(\omega) f(\delta_1, \delta_2)$], we find that $\hat{\rho}^{(1)} = 0$ is the only solution of Eq. (65), unless $\omega = \pm \omega_p$. Then, Eqs. (65) and (68) imply that

$$\hat{\rho}^{(1)} = \eta^+(\delta_1, \delta_2) \delta(\omega - \omega_p) + \eta^-(\delta_1, \delta_2) \delta(\omega + \omega_p). \tag{69}$$

Inserting Eq. (69) in Eq. (65), we obtain two uncoupled equations for η^+ and η^- . These can be solved by expanding η^\pm in Fourier series,

$$\eta^\pm(\delta_1, \delta_2) = \sum_{n=-\infty}^{\infty} \sum_{m=-\infty}^{\infty} (T^\pm)_n^m e^{in\delta_1} e^{im\delta_2}, \tag{70}$$

and solving the corresponding nonlinear systems of equations for the coefficients $(T^\pm)_n^m$. Once we obtain $(T^\pm)_n^m$, we can calculate $\hat{I}^{(1)}$ from Eq. (68). Notice that $\hat{\rho}^{(+\omega_p)} = \hat{\rho}^*(-\omega_p)$, by taking the complex conjugate in Eqs. (65) and (68). Then it follows from Eqs. (69) and (70) that

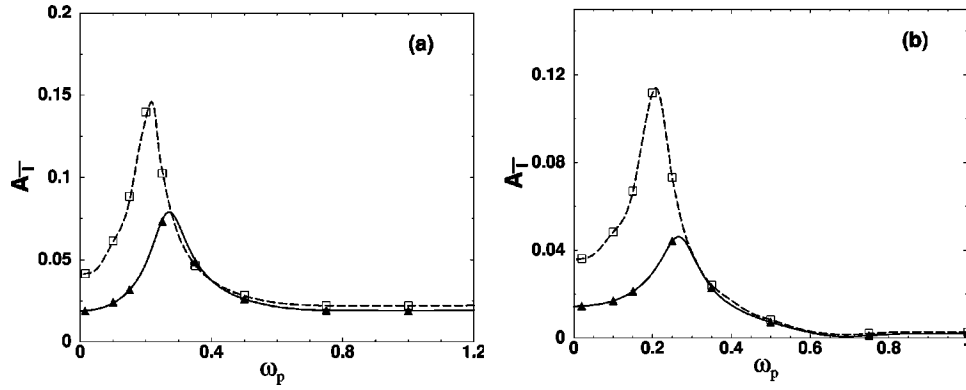


FIG. 12. Amplitude of the average screening current as function of ω_p . Comparison between the theoretical results and the numerical simulations, marked by symbols. Parameters are $D=0.05$, $\beta=1$, $J=0.4$, $\bar{M}=0.01$ (solid line for the theory, and solid triangle for the simulations), and $\bar{M}=0.05$ (dashed line for the theory, and open square for the simulations). (a) Flux-injected probe $\Phi_e^{(0)}=0.45$, $q=0.01$. (b) Current-injected probe $J_0=0.4$, $q=0.01$.

$(T^+)_n^m = ((T^-)_{-n}^{-m})^*$. Therefore, we conclude that $\hat{T}^{(1)}(-\omega_p) = (\hat{T}^{(1)})^*(+\omega_p)$, and the inverse Fourier transform yields

$$I^{(1)}(t) = 2 \operatorname{Re}[\hat{T}^{(1)}(\omega_p)] \cos(\omega_p t) - 2 \operatorname{Im}[\hat{T}^{(1)}(\omega_p)] \sin(\omega_p t). \quad (71)$$

Knowing $I^{(1)}(t)$, its amplitude can be readily computed and the result is

$$A_{\bar{I}} = 2 \sqrt{\hat{T}^{(1)}(\hat{T}^{(1)})^*} + O(\varepsilon^2). \quad (72)$$

In Fig. 12(a), we plot the numerical solution for two different values of the coupling and the theoretical approximation (72), showing a remarkable agreement with the theoretical results corresponding to the first-order expansion. It should be noticed, however, that the amplitude of the probe signal considered here is small, $q=0.01$. For increasing strength of the amplitude, higher orders in the expansion may be required. Once $\rho^{(1)}$ is known, it is also straightforward to find the successive terms in the expansion. Without entering into a detailed study, some general features can easily be drawn from the hierarchy of equations for $\rho^{(j)}$. Similarly to the analysis for $\hat{\rho}^{(1)}$, and by taking into account that $\hat{\rho}^{(1)}$ is a function exclusively of $\omega \pm \omega_p$, it is straightforward to prove that $\hat{\rho}^{(2)}=0$ is the only solution, unless $\omega=0, \pm 2\omega_p$. In general, successive terms will depend on higher harmonics of the main frequency ω_p .

We note that the probe signal could also be applied as an addition to the bias current (current injection), keeping the external flux Φ_{ex} constant. The resulting FPE may be solved in a manner analogous to the solution given above for the flux-injected case. We relegate the details to the Appendix, but show a comparison between the theory and numerical simulations in Fig. 12(b). Again, the agreement is remarkably good. Finally, we mention that it is also possible to calculate the frequency by analyzing the transition probabil-

ity in the FPE toward the stationary state, and thus to calculate the correlation function and its Fourier transform to obtain the power spectrum. However, extracting any analytical information from such an approach is quite involved. Furthermore, it might be possible to compute the frequency directly using Langevin simulations. However, for large noise levels, extracting the frequency from Langevin simulations would require averaging over many runs, making the FPE approach presented in this paper far more suitable.

VI. DISCUSSION

In this paper we have investigated the dynamics of an array of globally coupled SQUIDs. We have found that the coupling can lead to interesting effects. The main result is that the coupling strength determines the underlying (i.e., running) frequency of the system. For the deterministic case, this can be seen directly from the exact solution we have found. For the noisy case, this can be determined either via direct numerical simulations of the Langevin equations or via the investigation of the FPE we have derived.

As in other nonlinear systems, determining the underlying frequency can have practical applications. Unfortunately, for large noise levels, this task is generally very difficult. However, we have shown that the inclusion of a sinusoidal probe signal can be utilized to determine this frequency. In particular, we have found that the power spectrum of the experimentally relevant observable (the average screening current) displays a classical resonance phenomenon. As the frequency of the probe signal approaches the underlying frequency, the response gets amplified. Thus, the plot of response amplitude vs frequency shows a maximum at the underlying frequency. Noting that the underlying frequency is a function of the externally controllable bias parameters, we are now in a position to explain the resonance behavior observed in earlier experiments [12]. In these experiments, a time-sinusoidal probe signal was applied to a single dc SQUID, with the dc bias current and external magnetic flux used as deterministic laboratory control parameters. Past the onset of the saddle-node bifurcation, characterized by the experimental observa-

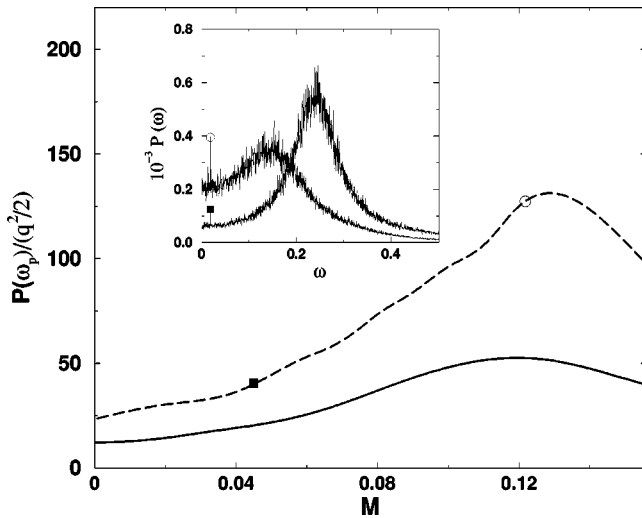


FIG. 13. Ratio between the peak in the power spectrum and the signal strength as a function of the coupling strength M for a system of two coupled SQUIDs. The signal frequency is $\omega_p = 0.018$ with an amplitude of $q = 0.01$ (solid line) and $q = 0.0025$ (dashed line). The inset shows the power spectrum for two different values of M ($M = 0.045$ for the closed square and $M = 0.122$ for the open circle). Other parameters as in Fig. 2.

tion of a phase diagram analogous to Fig. 1, we observed a local maximum in the local SNR measured at the probe frequency, for certain bias parameters. The noise in the experiment was not controlled externally, being assumed to arise from thermal noise in the junctions. Clearly, the results of this work indicate that such an effect occurs because, at a particular bias condition, the resulting spontaneous oscillation frequency matches the probe frequency, leading to a considerable decrease in the local dispersion (measured about the probe frequency). In fact, in our earlier work [2], we showed that at this resonance, the noise floor of the device was lowered across the output power spectrum, with the most striking effects appearing at the probe frequency and its harmonics. The results of this paper, while providing the basis for explaining the experimental observations, also show that the effect is more striking in a coupled array, when the coupling coefficient can, in fact, control the resonance via its effect on the underlying oscillation frequency.

The observed resonance phenomenon might be used to develop more sensitive SQUID-based measurement or quantification systems. Imagine trying to detect a weak sinusoidal target signal with an amplitude that is very small, perhaps even smaller than the noise level. If the target frequency is far removed from the underlying SQUID frequency this signal will be difficult to detect. However, by coupling SQUIDs and adjusting the coupling strength (or other control parameters if the coupling strength is inaccessible to adjustment) we can match the underlying frequency to the target frequency and increase the response dramatically.

This scenario is shown in Fig. 13 where we have plotted the amplification of the target signal, defined as the power at

the target frequency (output) divided by the power of the target signal (input), as a function of the coupling strength for $N=2$. The curves, for two different values of q , clearly show a typical resonance shape, indicating the presence of an optimal value of M . The inset of Fig. 13 shows the power spectrum for two different values of M . The peak values at ω_p are also plotted as symbols in the amplification curves. At the optimal value of the coupling strength, the target signal for the small value of q is amplified by more than 100, representing a dramatic increase in sensitivity of the SQUID. Note that in this example we have only used two SQUIDs, making this scenario experimentally plausible.

The results of this paper can be applied to other systems displaying bifurcations; in fact, an application of these ideas to the problem of noise-induced firing in type-I neurons is currently being actively explored [25] via an analysis of the Morris-Lecar model equations in the neighborhood of their saddle-node bifurcation, using center-manifold reduction theory. Note also that, in the single SQUID (as well as the Morris-Lecar neuron), one can approximate the dynamics near the onset of the bifurcation by simple “Integrate-and-fire” dynamics [2]. This representation is elegant; it provides a valuable tool for doing analytic calculations near the critical point, and it affords a case for the universality of such simplified dynamics close to the critical point. The procedure uses the already (via center-manifold theory) computed running frequency to set the width of the “bottleneck” (in the circle representation of the dynamics near the critical point), following which a linear Langevin equation is written down to describe the diffusion through the bottleneck with the noise added to the normal form. An analogous procedure for the coupled SQUID case is currently under investigation.

ACKNOWLEDGMENTS

This work was supported by the Office of Naval Research (Code 331). We also thank the National Partnership for Advanced Computational Infrastructure at the San Diego Supercomputer Center for computing resources, and acknowledge valuable discussions with Dag Winkler, Kurt Wiesenfeld, and Terry Clark.

APPENDIX: FPE SOLUTION FOR CURRENT-INJECTED PROBE SIGNAL

In a manner similar to the theory shown in Sec. V B, it is straightforward to analyze the case of a probe signal given by $J = J_0 + q \sin(\omega_p t)$, $q = \varepsilon Q$, where $\varepsilon \ll 1$. In the following, we shall illustrate the main differences. Inserting Eq. (53) into Eq. (40), we obtain now the following hierarchy of equations:

$$\frac{\partial \rho^{(0)}}{\partial \tau} = 0, \quad (\text{A1})$$

$$\begin{aligned} \frac{\partial \rho^{(1)}}{\partial \tau} = & D \left[\frac{\partial^2 \rho^{(0)}}{\partial \delta_1^2} + \frac{\partial^2 \rho^{(0)}}{\partial \delta_2^2} \right] \\ & - \frac{\partial}{\partial \delta_1} \left[\left(J - \nu - \sin \delta_1 + \frac{2\pi\bar{M}}{\beta\Phi_0} \bar{I}^{(0)} \right) \rho^{(0)} \right] \\ & - \frac{\partial}{\partial \delta_2} \left[\left(J + \nu - \sin \delta_2 - \frac{2\pi\bar{M}}{\beta\Phi_0} \bar{I}^{(0)} \right) \rho^{(0)} \right] \\ & - \frac{\partial \rho^{(0)}}{\partial t}, \end{aligned} \quad (\text{A2})$$

$$\begin{aligned} \frac{\partial \rho^{(2)}}{\partial \tau} = & D \left[\frac{\partial^2 \rho^{(1)}}{\partial \delta_1^2} + \frac{\partial^2 \rho^{(1)}}{\partial \delta_2^2} \right] - \frac{\partial}{\partial \delta_1} \left[(J - \nu - \sin \delta_1) \rho^{(1)} \right. \\ & \left. + \frac{2\pi\bar{M}}{\beta\Phi_0} (\bar{I}^{(0)} \rho^{(1)} + \bar{I}^{(1)} \rho^{(0)}) \right] - \frac{\partial}{\partial \delta_2} \left[(J + \nu \right. \\ & \left. - \sin \delta_2) \rho^{(1)} - \frac{2\pi\bar{M}}{\beta\Phi_0} (\bar{I}^{(0)} \rho^{(1)} + \bar{I}^{(1)} \rho^{(0)}) \right] - \frac{\partial \rho^{(1)}}{\partial t} \\ & - Q \sin(\omega_p t) \left[\frac{\partial \rho^{(0)}}{\partial \delta_1} + \frac{\partial \rho^{(0)}}{\partial \delta_2} \right]. \end{aligned} \quad (\text{A3})$$

In a manner analogous to the theory for the flux probe signal case, necessitated by the need to remove the secular terms, we obtain the following equations for $\rho^{(0)}$ and $\rho^{(1)}$:

$$\begin{aligned} D \left[\frac{\partial^2 \rho^{(0)}}{\partial \delta_1^2} + \frac{\partial^2 \rho^{(0)}}{\partial \delta_2^2} \right] - \frac{\partial}{\partial \delta_1} \left[\left(J - \nu - \sin \delta_1 + \frac{2\pi\bar{M}}{\beta\Phi_0} \bar{I}^{(0)} \right) \rho^{(0)} \right] \\ - \frac{\partial}{\partial \delta_2} \left[\left(J + \nu - \sin \delta_2 - \frac{2\pi\bar{M}}{\beta\Phi_0} \bar{I}^{(0)} \right) \rho^{(0)} \right] - \frac{\partial \rho^{(0)}}{\partial t} = 0, \end{aligned} \quad (\text{A4})$$

$$\begin{aligned} D \left[\frac{\partial^2 \rho^{(1)}}{\partial \delta_1^2} + \frac{\partial^2 \rho^{(1)}}{\partial \delta_2^2} \right] - \frac{\partial}{\partial \delta_1} \left[(J - \nu - \sin \delta_1) \rho^{(1)} \right. \\ \left. + \frac{2\pi\bar{M}}{\beta\Phi_0} (\bar{I}^{(0)} \rho^{(1)} + \bar{I}^{(1)} \rho^{(0)}) \right] - \frac{\partial}{\partial \delta_2} \left[(J + \nu \right. \\ \left. - \sin \delta_2) \rho^{(1)} - \frac{2\pi\bar{M}}{\beta\Phi_0} (\bar{I}^{(0)} \rho^{(1)} + \bar{I}^{(1)} \rho^{(0)}) \right] - \frac{\partial \rho^{(1)}}{\partial t} \\ - Q \sin(\omega_p t) \left[\frac{\partial \rho^{(0)}}{\partial \delta_1} + \frac{\partial \rho^{(0)}}{\partial \delta_2} \right] = 0. \end{aligned} \quad (\text{A5})$$

Fourier transforming Eq. (A5), we obtain

$$\begin{aligned} i\omega \hat{\rho}^{(1)} = & D \left[\frac{\partial^2 \hat{\rho}^{(1)}}{\partial \delta_1^2} + \frac{\partial^2 \hat{\rho}^{(1)}}{\partial \delta_2^2} \right] - \frac{\partial}{\partial \delta_1} \left[(J - \nu - \sin \delta_1) \hat{\rho}^{(1)} \right. \\ & \left. + \frac{2\pi\bar{M}}{\beta\Phi_0} (\hat{I}^{(0)*} \hat{\rho}^{(1)} + \hat{I}^{(1)*} \hat{\rho}^{(0)}) \right] - \frac{\partial}{\partial \delta_2} \left[(J + \nu \right. \\ & \left. - \sin \delta_2) \hat{\rho}^{(1)} - \frac{2\pi\bar{M}}{\beta\Phi_0} (\hat{I}^{(0)*} \hat{\rho}^{(1)} + \hat{I}^{(1)*} \hat{\rho}^{(0)}) \right] \\ & - i \frac{Q}{2} \left\{ \frac{\partial}{\partial \delta_1} [\hat{\rho}^{(0)}(\omega + \omega_p) - \hat{\rho}^{(0)}(\omega - \omega_p)] \right. \\ & \left. + \frac{\partial}{\partial \delta_2} [\hat{\rho}^{(0)}(\omega + \omega_p) - \hat{\rho}^{(0)}(\omega - \omega_p)] \right\}. \end{aligned} \quad (\text{A6})$$

Equation (A6) can be solved for $\hat{\rho}^{(1)}$ together with $\int_0^{2\pi} \int_0^{2\pi} d\delta_1 d\delta_2 \hat{\rho}^{(1)} = 0$. In Fig. 12(b) we show a comparison between the theoretical solution and the numerical simulation.

- [1] See, e.g., S. Strogatz, *Nonlinear Dynamics and Chaos* (Perseus Press, New York, 1994).
 [2] M. Inchiosa, V. In, A. Bulsara, K. Wiesenfeld, T. Heath, and M. Choi, Phys. Rev. E **63**, 066114 (2001).
 [3] A. Bulsara, K. Wiesenfeld, and M. Inchiosa, Ann. Physik **9**, 655 (2000).
 [4] M.J. Feldman, P.T. Parrish, and R.Y. Chiao, J. Appl. Phys. **46**, 4031 (1975); S.T. Vohra, L. Fabiny, and K. Wiesenfeld, Phys. Rev. Lett. **72**, 1333 (1994); S.T. Vohra and K. Wiesenfeld, Physica D **86**, 27 (1995).
 [5] M. Sherwin and A. Zettl, Phys. Rev. B **32**, 5536 (1985); K. Wiesenfeld and I. Satija, *ibid.* **36**, 2483 (1987).
 [6] See, e.g., P.H. Bryant, R. Movshovich, and B. Yurke, Phys. Rev. Lett. **66**, 2641 (1991); B. Derighetti, M. Ravani, R. Stoop, P. Meier, P. Brun, and R. Badii, *ibid.* **55**, 1746 (1985); G.

- Ahlers, M.C. Cross, P.C. Hohenberg, and S. Safran, J. Fluid Mech. **110**, 297 (1981); K. Wiesenfeld and N.F. Tufillaro, Physica D **26**, 321 (1987).

- [7] See, e.g., A. Barone and G. Paterno, *Physics and Applications of the Josephson Effect* (Wiley, New York, 1982); J. Clarke, in *The New Superconducting Electronics*, edited by H. Weinstock and R. Ralston (Kluwer Academic, Amsterdam, 1993); D. Koelle, R. Kleiner, F. Ludwig, E. Dankster, and J. Clarke, Rev. Mod. Phys. **71**, 631 (1999).
 [8] K. Wiesenfeld, A. Bulsara, and M. Inchiosa, Phys. Rev. B **62**, R9232 (2000).
 [9] For overviews see K. Wiesenfeld and F. Moss, Nature (London) **373**, 33 (1995); A. Bulsara and L. Gammaitoni, Phys. Today **49**(3), 39 (1996); L. Gammaitoni, P. Hänggi, P. Jung, and F. Marchesoni, Rev. Mod. Phys. **70**, 1 (1998).

- [10] M. Inchiosa, A. Bulsara, K. Wiesenfeld, and L. Gammaitoni, *Phys. Lett. A* **252**, 20 (1999).
- [11] M. Inchiosa and A. Bulsara, in *Stochastic and Chaotic Dynamics in the Lakes*, edited by D.S. Broomhead, E. Luchinskaya, P.V.E. McClintock, and T. Mullin (AIP, Melville, NY, 2000).
- [12] A. Hibbs, in *Applied Nonlinear Dynamics and Stochastic Systems Near the Millenium*, edited by James B. Kadtko and Adi Bulsara, AIP Conf. Proc. No. **411** (AIP, Woodbury, NY, 1997); A. Hibbs and B. Whitecotton, *Appl. Supercond.* **6**, 495 (1999); M. Inchiosa, A. Bulsara, A. Hibbs, and B. Whitecotton, *Phys. Rev. Lett.* **80**, 1381 (1998).
- [13] J.A. Acebrón, A.R. Bulsara, and W.-J. Rappel, *Europhys. Lett.* (to be published).
- [14] See e.g., M. Löcher, D. Cigna, E. Hunt, G. Johnson, F. Marchesoni, L. Gammaitoni, M. Inchiosa, and A. Bulsara, *Chaos* **8**, 604 (1998), and references therein.
- [15] J. A Acebrón, A.R. Bulsara, M.E. Inchiosa, and W.-J. Rappel, *Europhys. Lett.* **56**, 354 (2001).
- [16] D. Sigeti and W. Horsthemke, *J. Stat. Phys.* **54**, 1217 (1989).
- [17] S.R. Massanés and C.J. Pérez Vicente, *Int. J. Bifurcation Chaos Appl. Sci. Eng.* **9**, 2295 (1999); *Phys. Rev. E* **59**, 4490 (1999).
- [18] H. Risken, *The Fokker-Planck Equation: Methods of Solution and Applications* (Springer-Verlag, Berlin, 1984).
- [19] P. Jung, *Phys. Rep.* **234**, 175 (1993).
- [20] J.D. Crawford, *Rev. Mod. Phys.* **63**, 991 (1991).
- [21] R.C. Desai and R. Zwanzig, *J. Stat. Phys.* **19**, 1 (1978).
- [22] M. Shiino, *Phys. Lett.* **112A**, 302 (1985); *Phys. Rev. A* **36**, 2393 (1987).
- [23] P. Reimann, R. Kawai, C. Van den Broeck, and P. Hänggi, *Europhys. Lett.* **45**, 545 (1999).
- [24] For the single SQUID, we can prove rigorously that the only solution to the FPE is time independent [15].
- [25] A. Longtin, A. Bulsara, and C. Langevin (unpublished).